Safer-by-design biocides made of tri-thiol bridged silver nanoparticle assemblies

Marianne Marchioni, Giulia Veronesi, Isabelle Worms, Wai-Li Ling, Thomas Gallon, Didier Léonard, Christelle Gateau, Mireille Chevallet, Pierre-Henri Jouneau, Laura Carlini, et al.

Cite this: DOI: 10.1039/c9nh00286c

2019 Nanoscale Horizons

Published on 11 November 2019.

Received 1st May 2019,

Accepted 14th August 2019

Nanoscale Horiz. 2020 Mar 1;5(3):507-513

Safer-by-design biocide made of tri-thiol bridged silver nanoparticle assemblies

MARCHIONI,[a] Giulia VERONESI,[a,c] Isabelle WORMS,[a,d,≠] , Wai Li LING,[e] Thomas GALLON,[a,b] Didier LEONARD,[f] Christelle GATEAU,[b] Mireille CHEVALLET,[a] Pierre-Henri JOUNEAU,[g] Laura CARLINI,[h] Chiara BATTOCCHIO,[h] Pascale DELANGLE,[b] Isabelle MICHAUD-SORET,*[a] and Aurélien DENIAUD*[a]

a. Univ. Grenoble Alpes, CNRS, CEA, BIG-LCBM, 38000 Grenoble, France
E-mail: aurelien.deniaud@cea.fr; Tel : + 33 (0)4 38 78 96 51
E-mail: isabelle.michaud-soret@cea.fr; Tel : + 33 (0)4 38 78 99 40
b. Univ. Grenoble Alpes, CEA, CNRS, INAC-SYMMES, 38000 Grenoble, France
c. ESRF, The European Synchrotron. 71 avenue des Martyrs, 38000 Grenoble, France
d. Univ. Grenoble Alpes, CEA, LITEN/DTNM/SEN/L2N, F-38054 Grenoble Cedex 09, France

e. Univ. Grenoble Alpes, CEA, CNRS, IBS, F-38000 Grenoble, France
f. Univ Lyon, CNRS, Université Claude Bernard Lyon 1, Institut des Sciences Analytiques, UMR 5280, 5, rue de la Doua, F-69100 Villeurbanne, France
g. Univ. Grenoble Alpes, CEA, INAC-MEM, 38000 Grenoble, France
h. Univ. Roma Tre, Dept. of Sciences, Via della Vasca Navale 79 - 00146 - Rome, Italy
≠ Present address: Department F.-A. Forel for Environmental and Aquatic sciences, University of Geneva, 66 boulevard Carl Vogt CH-1211 Geneva 4.
† Electronic Supplementary Information (ESI) available: See DOI: 10.1039/x0xx00000x

Abstract

Silver nanoparticles (AgNPs) are efficient biocide increasingly used in consumer products and medical devices. Their activity is due to their capacity to release bioavailable Ag(I) ions making them a long-lasting biocide but AgNPs themselves are usually easily released from the product. Besides, AgNPs are highly sensitive to various chemical environment that triggers their transformation, decreasing their activity. Altogether, AgNPs widespread use leads to bacterial resistance and safety concerns for Human and the environment. There is thus a crucial need for improvements. Herein, a proof of concept for a novel biocide based on AgNP assemblies bridged together by tri-thiol bioinspired ligand is presented. The final nanomaterial is stable and less sensitive to chemical environment with AgNPs completely covered by organic molecules tightly bound via their thiol functions. Therefore, these AgNP assemblies can be considered as safer-by-design and innovative biocides, since they deliver sufficient Ag(I) amount for biocidal activity with no release of AgNPs, which are insensitive to transformations in the nanomaterial.

Introduction

Silver nanoparticles (AgNPs) are widely used in consumer products for their biocidal activity. AgNP-containing medical devices is also a growing market with applications in dentistry, prosthesis, catheters or wound dressings. Their action is due to Ag(I) release that is highly toxic for microorganisms inducing alterations of lipid bilayers, proteins and nucleic acids. This wide spectrum of effects makes them a good choice to avoid specific mutations in bacterial strains that could confer resistance. However, resistant strains have been observed[1] thanks to acquisition of the ability to chelate and excrete or to trap Ag species.[2–4] The reactivity of Ag in general and AgNPs in particular is very complex and depends on the surrounding media[5] including living species such as *Bacillus subtilis* that secretes molecules to hinder their activity.[6] Ag(I) release from AgNPs is based on an oxidative dissolution mechanism and thus requires oxygen.[7] In aerobiosis, the metallic Ag(0) core of AgNPs is covered by surface Ag(I) species, and the dissolution of the NP into ions is favored by pH decrease[8] and/or by some thiol molecules.[9,10] The behavior of AgNPs in presence of thiol molecules is highly versatile either inducing time-dependent dissolution into ions[9,10] or forming a coating that protects the NP.[8,11] These phenomena depend on the architecture of the molecules and the number of thiols[8,9,11] but remains unpredictable to date. In order to solve concerns about NP use, next generation nanomaterials are being developed following a safer-by-design approach.[12] In the case of AgNPs, it is crucial to limit Ag(I) release to the strictly required amount for the biocidal activity. Besides, it would also be interesting to avoid AgNP release from the product in the environment or in the human body for medical devices. This approach would therefore limit bacterial resistance against silver and toxicity for mammals and other living species. In order to reach these objectives, we developed an innovative strategy that consists in bridging AgNPs together using a tri-thiol molecule, which favors the formation of larger and stable species that we decided to

name_AgNP assemblies. In these assemblies, AgNPs keep their high specific surface area without being released from the final product. The growth of the AgNP assemblies is mediated by thiol functions and can be controlled using a thiol-reactive molecule to stop the process and thereby to obtain a stable nanomaterial of defined size. Hence, AgNPs are entrapped into a tightly bound organic coating, which enables the long-lasting, slow dissolution into Ag(I). Therefore, the release from AgNP assemblies is reduced to an amount necessary to keep the biocidal activity, unlike isolated AgNPs, which undergo uncontrolled ion release. Altogether, using a smart and innovative process we reached the objectives needed for the future production of safer biocides to be grafted on nano-enabled biocidal products.

Results and discussion

$NTA(CysOEt)_3$, abbreviated L^{3S} in the following, is a tri-thiol molecule with C_3 symmetry inspired from a single metallothionein Cu(I) binding site (Fig. 1a).[13] This is a high affinity ligand for Cu(I) and Ag(I) that forms AgS_3 complexes.[14] In the presence of 20 nm diameter citrate-coated AgNPs in equimolar concentration of Ag and S, L^{3S} induced a change of the solution color over time (Fig. 1b), due to a modification of the surface plasmon resonance (SPR) properties (Fig. 1c). Indeed, a decrease of the specific AgNP SPR signal around 400 nm was observed, along with the appearance of a broad peak centered at higher wavelengths that increased with time. This phenomenon is explained by the formation of non-symmetric dipole and is due to nanoparticles in contact without interpenetration between them.[15] These results suggested that L^{3S} induced an AgNP agglomeration-like mechanism, which is confirmed by the time-dependent increase of the hydrodynamic diameter of the species in solution, reaching about 250 nm with an homogenous distribution after 1h of reaction and more than 1 µm in an heterogeneous distribution after 75 min (Fig. 1d). However, several experimental evidences allow us to rule out the occurrence of simple agglomeration, meant as the formation of clusters of NPs held together by weak physical interactions in an unpredictable way, and resulting in a bulk material with no nano-properties.

Thiol molecules were previously demonstrated to favor AgNP dissolution into Ag(I) soluble species with a kinetic increasing with the number of thiol per molecule.[9] Indeed, phytochelatin-3, a tri-thiol molecule, induced an almost four times faster dissolution than glutathione, our standard one thiol molecule. Surprisingly, similar experiments performed with the tri-thiol molecule L^{3S} showed a slightly slower AgNP dissolution compared to the reaction with glutathione leading to lower amount of Ag(I) released after 24h incubation (Fig. 1e). In order to have a complete view of the different species produced over time, asymmetrical flow-field flow-fractionation (AF_4) experiments were performed with online detection of Ag by inductively coupled plasma – mass spectrometry (ICP-MS) (Fig. 1f). Pristine AgNPs alone are eluted at 15 min retention time and remained stable in solution over 24h. The incubation with L^{3S} led to i) the decrease of AgNP peak (15 min) over time, ii) the appearance of a peak at lower retention time around 11 min that corresponds to Ag(I) soluble species and iii) the appearance of a broad peak corresponding to assemblies at a higher retention time, the latter increasing with the incubation duration. These results highlight the time-dependent

formation of large assemblies of AgNPs triggered by L^{3S}. Moreover, the kinetics of the process can gradually be slowed down by decreasing the S to Ag molar ratio to 0.25 and 0.05, as shown by SPR spectra and dynamic light scattering (DLS) distributions (Fig. S1, ESI†). To control the assembly process, further experiments were performed with an S to Ag molar ratio of 0.25 and using iodoacetamide, a thiol-reactive molecule that alkylates and blocks free thiol functions. When added after 1h incubation between AgNPs and L^{3S}, the evolution of both SPR spectra and DLS distributions were stopped and the assemblies were stable for at least 120h at 25°C (Fig. 2a-b *vs* Fig. 1c-d). This proves that the AgNP assembly is thiol-driven and is not an agglomeration mechanism, which would be insensitive to iodoacetamide but sensitive to dilution, as observed with oxidized glutathione (Fig. S2, ESI†).

In order to prepare assemblies of different sizes, L^{3S} and AgNPs were incubated during 1 hour before addition of iodoacetamide. Thiol-blocked AgNP assemblies were then fractionated over discontinuous sucrose gradient centrifugation into assemblies of different average hydrodynamic diameters (Fig. 2c). We obtained populations of assemblies of 40, 60 and 200 nm based on DLS measurement with different SPR spectra and colors (Fig. S3, ESI†) and zeta potentials of -28.3, -21.0 and -24.8 mV for the assemblies of 40, 60 and 200 nm, respectively. The DLS diameter distributions showed a clear shift towards larger diameter for the main peak but a second low intensity peak was observed at smaller values for both 60 and 200 nm assemblies (Fig. 2c). Therefore, the diameters determined by DLS are not accurate and the values 40, 60 and 200 nm are used as labels of the different population of assemblies in the following. The morphology of the assemblies and the number of particles per assembly were analyzed by electron microscopy: scanning transmission electron microscopy (STEM) and cryo-transmission electron microscopy (cryo-TEM) (Fig. 2d and S4, ESI†). Despite the different preparation protocols, both techniques clearly showed clusters of AgNPs comprising a number of NPs that increased with the expected size of the assemblies. Statistical analysis (Fig. S4b) showed that 40 nm assemblies are mainly formed by 1 to 4 NPs, 60 nm assemblies contained between 5 and 40 NPs with most assemblies containing 15 NPs and 200 nm assemblies are made of 16 to 60 NPs with most assemblies containing 40. Indeed, the larger is the hydrodynamic diameter of an assembly the more diverse are the possibilities to make it. Cryo-TEM also showed very short distances between AgNPs within an assembly, which is consistent with the small size of L3S with maximum distances between two sulfur atoms in the nanometer range (Fig. 2d and S4c).

Thiols are at the core of the assembly mechanism; therefore, we probed sulfur bonds with synchrotron radiation – induced X-ray photoelectron spectroscopy (SR-XPS) on assemblies of small (40 nm diameter) and medium (80 nm diameter) sizes (Fig. 3). Between 56 and 64% of the sulfur atoms were found to be bound to Ag atoms at the NP surface, with two distinct geometries in similar proportions. S 2p3/2 components at binding energies (BE) about 161 eV and 162 eV are attributed to sulfur atoms covalently bonded to metals in a monolayer or sub-monolayer regime, with the S atom in two different hybridizations, sp (161.3 eV) and sp3 (162.1 eV),16,17 coherently with what was already observed for organic thiols chemisorbed onto gold surfaces.18 The low BE signal is reported as occurring characteristically in self-assembling monolayers of low degree of coverage.19 Indeed, hybridization change is likely to cause a peak shift,20 with a BE of 162.1 eV for a sp3 S atom, a BE of about 161.3 eV (nearly 1 eV lower) would be expected for an sp-hybridized S atom.20 This proves the direct binding of the thiolate functions of L3S to the AgNP with two different geometries, linear and angular, corresponding to sp and sp3 hydridization, respectively (Scheme S1, ESI†).20,21 Due to iodoacetamide reaction, 25 to 29% of the sulfur atoms were involved in bonds with carbon (thioethers), while the remaining 10 to 15% formed disulfide bridges. This minor fraction of S species might belong to L3S molecules grafted to the NP surface with two thiolate groups, whereas the third thiolate forms an S-S bond with another partially grafted L3S molecule. Besides, the absence of a signal component below 161 eV suggests that the assemblies do not contain silver sulfide.22,23 XPS Ag 3d spectra showed that the fraction of Ag(I) remained constant around 6.6-6.8% of total Ag in the assemblies (Fig. S5, ESI†), which is close to the expected proportion of surface Ag for a 20 nm diameter NP (5.8%) confirming the limited dissolution of AgNPs. Therefore, AgNP assemblies are thiol-mediated and their structure is stabilized by Ag-S bonds involving L3S that has the capability to bridge AgNPs thanks to its three thiol functions in a tripodal architecture. Besides, ToF-SIMS positive mode analysis enabled the detection of significant amounts of Ag atoms (both isotopes 107 and 109, Fig. S6, ESI†) for citrate-coated AgNPs but not for AgNP assemblies of 40 or 200 nm. Since ToF-SIMS information depth is limited to the first monolayers at the surface of the sample, these results showed that L3S forms a layer that completely covers AgNPs in the assemblies.

The biological activity of assemblies of different diameters was then compared with citrated-coated AgNPs in order to gain insights into their potential as biocide and their toxicity for Human. All assemblies possess antibacterial activity against Escherichia coli (Gram-negative), with minimal inhibitory concentration (MIC) of 5.2, 5.9 and 12.7 µM Ag for 40, 60 and 200 nm assemblies, respectively. These values are higher than those measured for citrate-coated 20 to 60 nm AgNPs

(MIC between 0.7 and 2.9 µM) (Fig. 4a), but still much lower than the values reported in literature for GSH-capped AgNPs (139 µM).24 The biocidal activity was also tested against a Gram-positive bacteria, Bacillus subtilis, known to be difficult to be killed by AgNPs notably because of its ability to modify AgNP surface.6,25 As expected, the Ag concentration required to observe a growth delay was much higher than for E. coli: 113, 138 and 33 µM for assemblies of 40, 60 and 200 nm, respectively.

Very interestingly, these concentrations are lower than the values determined for citrate-coated AgNPs (260 µM) (Fig. 4a). Therefore, the thick and tight coating afforded by the tri-thiol molecule L3S may protect assemblies against AgNP surface modifications that could prevent biocidal activity, rendering our assemblies more robust. Besides, toxicity was assessed in the human hepatocarcinoma cell line HepG2 since AgNPs accumulate in liver.26 We were not able to reach a significantly toxic concentration (200 µM Ag higher concentration tested) for any of the assemblies, while the lethal dose for 50% of the cells is about 75 µM for citrate-coated AgNPs (Fig. 4b and S7, ESI†). Therefore, AgNP assemblies possess a biocidal activity against diverse strains but their cytotoxicity for eukaryote cells is drastically decreased.

Conclusions

In conclusion, we described an assembly mechanism of AgNPs bridged together by a bio-inspired tri-thiol molecule. This process, driven by thiol binding to surface Ag(I), results in the formation of a scaffold that protects the NPs from massive transformations induced by various environmental conditions normally responsible for their fast dissolution, sulfidation or agglomeration (see review 5). Moreover, these architectures do not prevent Ag(I) release and only slow it down (Fig. 4c), providing a nanomaterial that can be regarded as a novel promising safer-by-design biocide. Its tunable and controlled ion release and low sensitivity to the surrounding medium make it a long-lasting biocide with drastically reduced hazard for Human and the environment with respect to currently employed technologies. The controlled Ag(I) release cannot only be explained by surface coverage since PVP-coated AgNPs are more toxic for prokaryotes and eukaryotes than assemblies.27 Therefore, the mixed sp3-sp hydridization of L3S thiols bound to surface Ag is likely to be responsible for the particular behavior of AgNPs involved in assemblies. The two hybridizations

could mirror ligand binding on two different chemisorption sites, as hollow and on-top sites that favor stabilization of the assembly and dissolution into ions, respectively.16,28

The current work therefore describes the proof of concept for the development of novel biocidal AgNP assemblies. An original nanomaterial with promising properties has been developed thanks to a tripodal tri-thiol molecule, whose thiolate functions interact with surface Ag(I) ions, thereby bridging the NPs. Finally, further development of the organic molecule will enable the covalent grafting of the assemblies into objects that require efficient and long-lasting biocide such as medical devices.

Experimental section

Experimental details are available in the ESI†.

Conflicts of interest

There are no conflicts to declare

Acknowledgements

The authors acknowledge Cécile Lelong for providing the B. subtilis strain, Delphine Truffier-Boutry for providing access to the AF4 instrument and Elisabeth Mintz for discussions. This work was funded by the CEA-Toxicology Transversal Program through the NanoSilverSol grant and by the CEA Transversal Programs Toxicology and Nanoscience through the NanoTox-RX grant. This research is part of the LabEx SERENADE (grant ANR-11-LABX-0064) and the LabEx ARCANE and CBH-EUR-GS (grant ANR-17-EURE-0003). MM and IW were supported by the LabEx SERENADE. The authors also acknowledge Alejandro Fernandez Martinez for its help with Zêta potential measurements that have been performed within the analytical platform of ISTerre (OSUG-France). The AF4-ICP-MS and NanoZS were funded by the EQUIPEX NanoID (grant ANR-10-EQPX-39-01). This work is also supported by the Université Grenoble Alpes – AGIR grant NanoSilverSafe and IRS NanoBIS grant. This work used the electron microscope platform of the Grenoble Instruct-ERIC Center (ISBG: UMS 3518 CNRS-CEA-UGA-EMBL) with support from FRISBI (ANR-10-INBS-05-02) and GRAL (ANR-10-LABX-49-01) within the Grenoble Partnership for Structural Biology (PSB). The EM facility is supported by the Auvergne-Rhône-Alpes Region, the Fondation Recherche Medicale (FRM), the fonds FEDER and the GIS-Infrastrutures en Biologie Sante et Agronomie (IBISA). We thank Dr. Guy Schoehn for support and access to the EM platform.

Author contributions

AD, IMS, PD and MM designed the study and interpreted the data. AD, GV, PD, IMS and MM wrote the paper. GV, IW and CB participated in data interpretation. MM, TG and IW characterized assembling process and prepared AgNP assemblies. IW performed AF4-ICP-MS experiments and interpreted the data. WLL performed cryo-TEM experiments including grid preparation. DL performed and analyzed ToF-SIMS experiments. CG synthesized the molecule L3S. CB, LC, GV and MM participated in synchrotron XPS experiments, data acquisition and analysis, and interpretation of the results. PHJ and MM performed STEM experiments and analysis. MM and MC performed cellular experiments. MM and AD performed biocidal experiments.

Notes and references

1 C. Gunawan, C. P. Marquis, R. Amal, G. A. Sotiriou, S. A. Rice and E. J. Harry, ACS Nano, 2017, 11, 3438–3445.

2 C. Haefeli, C. Franklin and K. Hardy, J. Bacteriol., 1984, 158, 389–392.

3 S. Silver, FEMS Microbiol. Rev., 2003, 27, 341–353.

4 S. Silver, A. Gupta, K. Matsui and J.-F. Lo, Met.-Based Drugs, 1999, 6, 315–320.

5 M. Marchioni, P.-H. Jouneau, M. Chevallet, I. Michaud-Soret and A. Deniaud, Coord. Chem. Rev., 2018, 364, 118–136.

6 E. Eymard-Vernain, Y. Coute, A. Adrait, T. Rabilloud, G. Sarret and C. Lelong, PLOS ONE, 2018, 13, e0197501.

7 J. Liu and R. H. Hurt, Environ. Sci. Technol., 2010, 44, 2169–2175.

8 J. Liu, D. A. Sonshine, S. Shervani and R. H. Hurt, ACS Nano, 2010, 4, 6903–6913.

9 M. Marchioni, T. Gallon, I. Worms, P.-H. Jouneau, C. Lebrun, G. Veronesi, D. Truffier-Boutry, E. Mintz, P. Delangle and A. Deniaud, Environ. Sci. Nano, 2018, 5, 1911–1920.

10 L. Sigg and U. Lindauer, Environ. Pollut., 2015, 206, 582–587.

11 F. Porcaro, L. Carlini, A. Ugolini, D. Visaggio, P. Visca, I. Fratoddi, I. Venditti, C. Meneghini, L. Simonelli, C. Marini, W. Olszewski, N. Ramanan, I. Luisetto and C. Battocchio, Materials, 2016, 9, 1028.

12 J. Y. Bottero, J. Rose, C. de Garidel, A. Masion, T. Deutsch, G. Brochard, M. Carrière, N. Gontard, H. Wortham, T. Rabilloud, B. Salles, M. Dubosson, B. Cathala, D. Boutry, A. Ereskovsky, C. Auplat, L. Charlet, T. Heulin, E. Frejafon and S. Lanone, Environ. Sci. Nano, 2017, 4, 526–538.

13 A. M. Pujol, C. Gateau, C. Lebrun and P. Delangle, J. Am. Chem. Soc., 2009, 131, 6928–6929.

14 G. Veronesi, T. Gallon, A. Deniaud, B. Boff, C. Gateau, C. Lebrun, C. Vidaud, F. Rollin-Genetet, M. Carrière, I. Kieffer, E. Mintz, P. Delangle and I. Michaud-Soret, Inorg. Chem., 2015, 54, 11688–11696.

15 H. Cha, D. Lee, J. H. Yoon and S. Yoon, J. Colloid Interface Sci., 2016, 464, 18–24.

16 I. Venditti, G. Testa, F. Sciubba, L. Carlini, F. Porcaro, C. Meneghini, S. Mobilio, C. Battocchio and I. Fratoddi, J. Phys. Chem. C, 2017, 121, 8002–8013.

17 F. Mochi, L. Burratti, I. Fratoddi, I. Venditti, C. Battocchio, L. Carlini, G. Iucci, M. Casalboni, F. De Matteis, S. Casciardi, S. Nappini, I. Pis and P. Prosposito, Nanomaterials, 2018, 8, 488.

18 S. Ramsaywack, S. Martić, S. Milton, L. Gates, A. S. Grant, M. Labib, A. Decken and H.-B. Kraatz, J. Phys. Chem. C, 2012, 116, 7886–7896.

19 T. Ishida, M. Hara, I. Kojima, S. Tsuneda, N. Nishida, H. Sasabe and W. Knoll, Langmuir, 1998, 14, 2092–2096.

20 A. J. Leavitt and T. P. Beebe Jr, Surf. Sci., 1994, 314, 23–33.

21 T. Ishida, N. Choi, W. Mizutani, H. Tokumoto, I. Kojima, H. Azehara, H. Hokari, U. Akiba and M. Fujihira, Langmuir, 1999, 15, 6799–6806.

22 C. Battocchio, C. Meneghini, I. Fratoddi, I. Venditti, M. V. Russo, G. Aquilanti, C. Maurizio, F. Bondino, R. Matassa and M. Rossi, J. Phys. Chem. C, 2012, 116, 19571–19578.

23 A. V. Naumkin, A. Kraut-Vass, S. W. Gaarenstroom and C. J. Powell, There No Corresp. Rec. This Ref.

24 E. Amato, Y. A. Diaz-Fernandez, A. Taglietti, P. Pallavicini, L. Pasotti, L. Cucca, C. Milanese, P. Grisoli, C. Dacarro, J. M. Fernandez-Hechavarria and V. Necchi, Langmuir, 2011, 27, 9165–9173.

25 K. Rafińska, P. Pomastowski and B. Buszewski, Sci. Total Environ.

26 M. van der Zande, R. J. Vandebriel, E. Van Doren, E. Kramer, Z. Herrera Rivera, C. S. Serrano-Rojero, E. R. Gremmer, J. Mast, R. J. B. Peters, P. C. H. Hollman, P. J. M. Hendriksen, H. J. P. Marvin, A. A. C. M. Peijnenburg and H. Bouwmeester, ACS Nano, 2012, 6, 7427–7442.

27 G. Veronesi, A. Deniaud, T. Gallon, P.-H. Jouneau, J. Villanova, P. Delangle, M. Carrière, I. Kieffer, P. Charbonnier, E. Mintz and I. Michaud-Soret, Nanoscale, 2016, 8, 17012–17021.

28 H. Sellers, A. Ulman, Y. Shnidman and J. E. Eilers, J. Am. Chem. Soc., 1993, 115, 9389–9401.

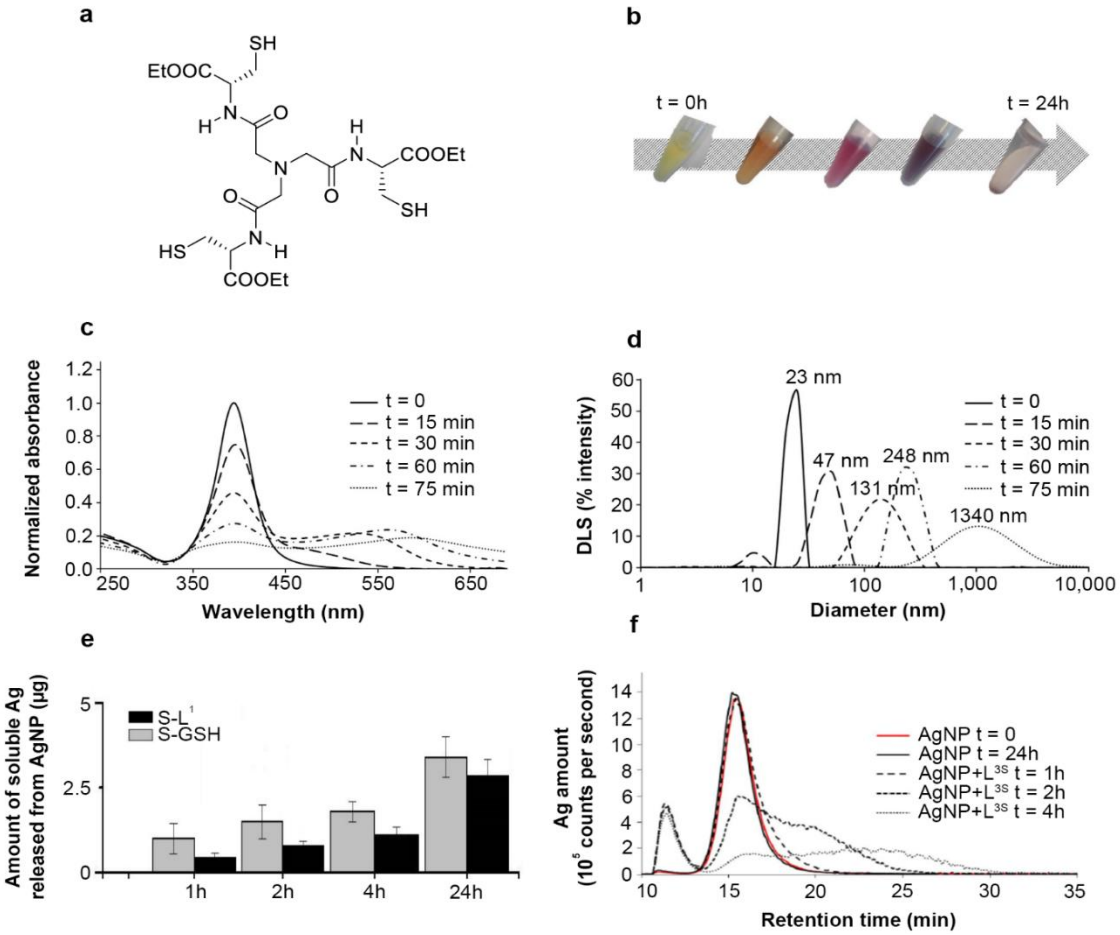

Fig. 1 L^{3S}-induced AgNP assemblies. (a) chemical structure of the tripodal molecule L^{3S}. (b) time-dependent evolution of the color of AgNP- L^{3S} mixture between 0 and 24 hours. (c) time-dependent analysis of AgNP SPR spectra in the presence of L^{3S} between 0 and 75 min of incubation in 1:1, S:Ag molar ratio. (d) time-dependent evolution of the hydrodynamic diameter distribution of the species in a solution containing AgNP and L^{3S} at a 1:1, S:Ag molar ratio and between 0 and 75 min of incubation. The average diameter is written on top of each peak. (e) AgNP dissolution into Ag(I) species in the presence of GSH (noted "S-GSH") or L^{3S} (noted "S- L^{3S}"). Time-dependent measurement of the amount of Ag into the soluble fraction determined by ICP-AES. This amount corresponds to the fraction of the sample recovered in the supernatant of the sucrose cushion centrifugation (see experimental section in ESI†). (f) AF_4 analysis of AgNPs in the presence of L^{3S}. Fractograms of species from AgNPs incubated alone for 0 or 24 hours and with L^{3S} for 1, 2 or 4 hours. The detection is based on ^{107}Ag by ICP-MS. In all experiments, t=0 corresponds to the AgNP alone in solution.

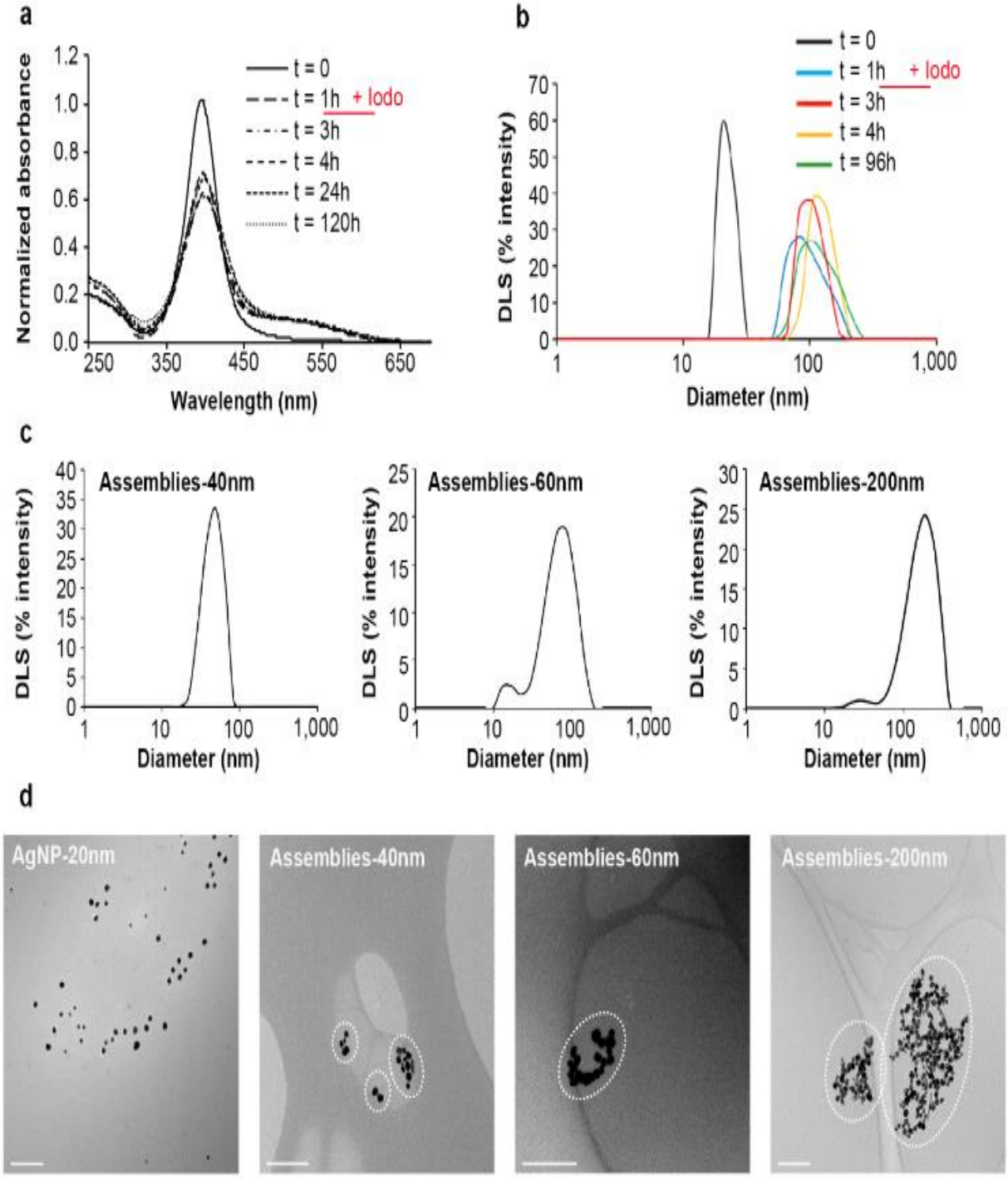

Fig. 2 AgNP assemblies: production, purification and characterization. (a) time-dependent analysis of AgNP SPR spectra in the presence of L^{3S} between 0 and 120 hours of incubation in 0.25:1, S:Ag molar ratio. The reaction between AgNPs and L^{3S} occurs during 1 hour, then iodoacetamide is added at 100 µM for a thiol concentration of 90 µM. SPR spectra were acquired up to 120 hours total incubation time. (b) in a set-up similar to (a), hydrodynamic diameter distribution of the species in solution were determined for the AgNPs alone (t=0), at t=1h (time for the addition of iodoacetamide) and then at t=3, 4 and 96 hours. (c) hydrodynamic diameter distribution of different populations of assemblies separated on discontinuous sucrose gradient centrifugation. Three different populations were recovered: ‘‘Assemblies-40nm’’ corresponds to assemblies of 40 nm average diameter by DLS, ‘‘Assemblies-60nm’’ corresponds to assemblies of 60 nm average diameter by DLS and ‘‘Assemblies-200nm’’ corresponds to assemblies of 200 nm average diameter by DLS. (d) analysis by cryo-TEM of the different population of assemblies compared to initial AgNPs, for which a proper dispersion on the grid is obtained. Assemblies constituted of larger number of particles with larger diameter of the assemblies were observed on the grids. Clusters of AgNPs considered as an assembly are encircled to help the understanding of our statistical analysis (Fig. S4b, ESI†). The scale bar corresponds to 200 nm. “Iodo” stands for iodoacetamide.

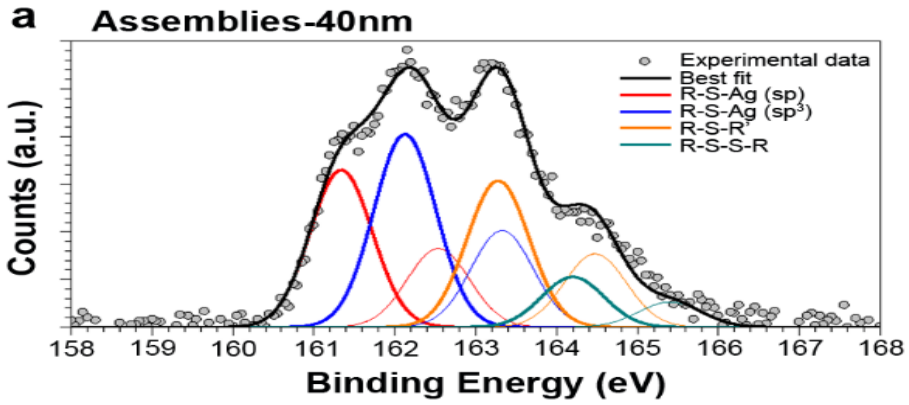

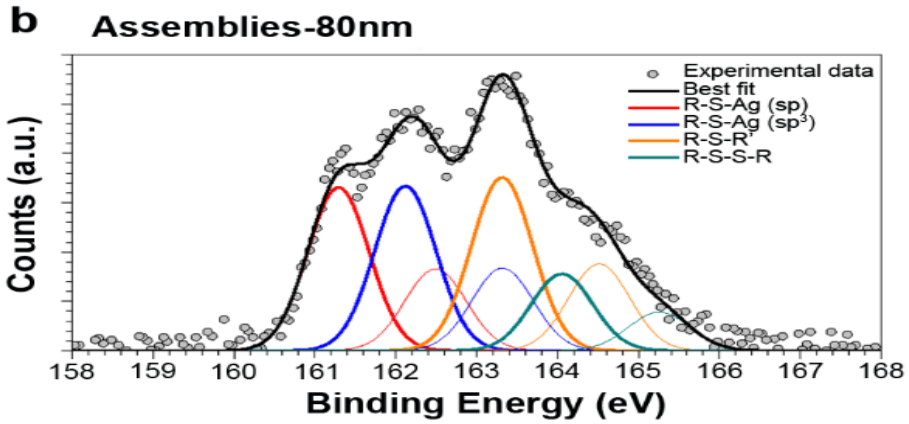

c

Assemblies	S2p$_{3/2}$ BE (eV)	FWHM (ev)	Atomic %*	Assignment
40 nm	161.33	0.83	29.4	**RS-Ag (sp)
	162.11	0.83	35.4	**RS-Ag (sp^3)
	163.20	0.83	24.8	RSR'
	163.92	0.83	10.4	RS-SR
80 nm	161.30	0.86	28.0	RS-Ag (sp)
	162.12	0.86	28.6	RS-Ag (sp^3)
	163.29	0.86	29.1	RSR'
	164.00	0.86	14.3	RS-SR

Fig. 3 Characterization of AgNP – L[3S] interaction. SR-XPS S 2p core-level spectra collected on 40nm AgNP assemblies (a) and 80nm AgNP assemblies (b). For each signal, two spin-orbit components are reported: S 2p$_{3/2}$ (thick curve) and S 2p$_{1/2}$ (thin curve), with fixed intensity ratio S 2p$_{3/2}$ / S 2p$_{1/2}$ = 2/1 and doublet separation 1.2 eV. (c) spectral assignment based on BE values of S 2p$_{3/2}$ components and semiquantitative analysis resulting in the estimation of the relative amount of the identified S species. * the statistic error in semiquantitative XPS analysis is of about 5% of the estimated value,[23] ** as reported in [16,19,20,22,24–26].

a

Diameter (nm)	Object type	MIC – *E. coli* (µM Ag)	Growth delay – *B. subtilis* (µM Ag)
20	NP	0.7 +/- 0.0	260 +/- 89
40	NP	0.7 +/- 0.0	-
60	NP	2.9 +/- 0.0	-
40	Assemblies	5.2 +/- 3.2	113 +/- 75
60	Assemblies	5.9 +/- 3.6	138 +/- 48
200	Assemblies	12.7 +/- 1.0	33 +/- 14

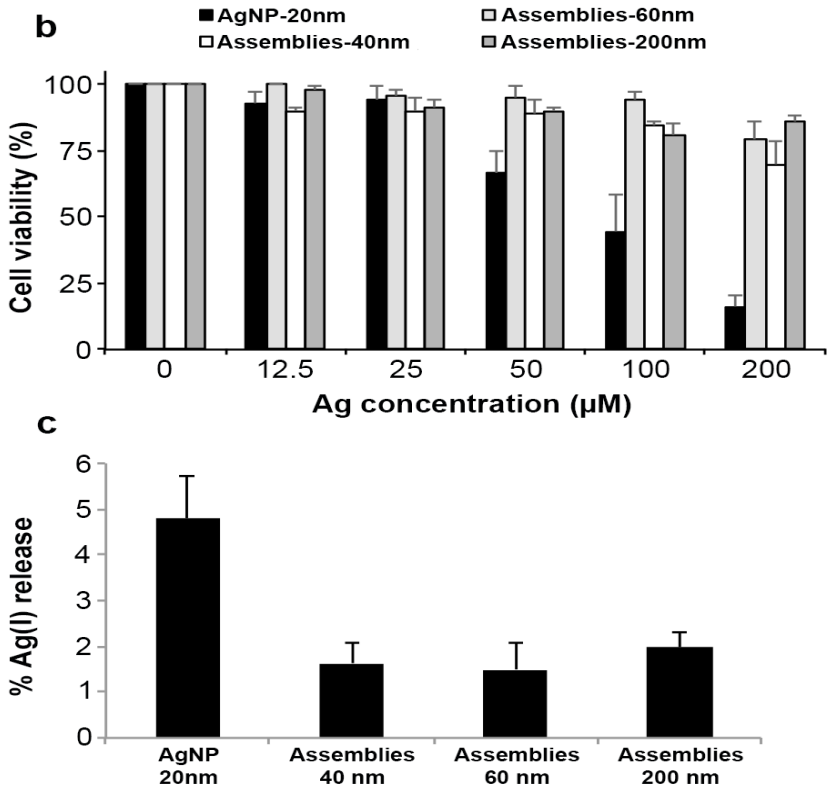

Fig. 4 Biological activity of AgNPs *versus* assemblies. (a) table presenting the MIC for AgNPs and the different assemblies determined based on overnight growth in liquid minimal media for *E. coli* and the concentration inducing growth delay in LB medium for *B. subtilis*. (b) HepG2 cell viability. Hepatocytes were exposed to 20 nm citrate-coated AgNPs or assemblies of 40, 60 or 200 nm for 24h before being harvested. Total and viable cells were counted in a TC20 Automated Cell Counter (Bio-Rad) using Trypan Blue. (c) amount of Ag(I) released from AgNPs or assemblies in 10 days. Each sample diluted in HEPES-citrate buffer at 370 µM in Ag was incubated for 10 days at 25 °C with constant steering at 400 rpm. The mixtures were separated on sucrose cushion centrifugation. Ag soluble species were in the supernatant and were quantified by ICP-AES. All the experiments were carried out at least three times independently.

Supplementary Information

Safer-by-design biocide made of tri-thiol bridged silver nanoparticle assemblies

Marianne MARCHIONI,[a] Giulia VERONESI,[a,c] Isabelle WORMS,[a,d,≠] , Wai Li LING,[e] Thomas GALLON,[a,b] Didier LEONARD,[f] Christelle GATEAU,[b] Mireille CHEVALLET,[a] Pierre-Henri JOUNEAU,[g] Laura CARLINI,[h] Chiara BATTOCCHIO,[h] Pascale DELANGLE,[b] Isabelle MICHAUD-SORET,*[a] and Aurélien DENIAUD*[a]

[a] Univ. Grenoble Alpes, CNRS, CEA, BIG-LCBM, 38000 Grenoble, France

[b] Univ. Grenoble Alpes, CEA, CNRS, INAC-SYMMES, 38000 Grenoble, France

[c] ESRF, The European Synchrotron. 71 avenue des Martyrs, 38000 Grenoble, France

[d] Univ. Grenoble Alpes, CEA, LITEN/DTNM/SEN/L2N, F-38054 Grenoble Cedex 09, France

[e] Univ. Grenoble Alpes, CEA, CNRS, IBS, F-38000 Grenoble, France

[f] Univ Lyon, CNRS, Université Claude Bernard Lyon 1, Institut des Sciences Analytiques, UMR 5280, 5, rue de la Doua, F-69100 Villeurbanne, France

[g] Univ. Grenoble Alpes, CEA, INAC-MEM, 38000 Grenoble, France

[h] Univ. Roma Tre, Dept. of Sciences, Via della Vasca Navale 79 - 00146 - Rome, Italy

[≠] Present address: Department F.-A. Forel for Environmental and Aquatic sciences, University of Geneva, 66 boulevard Carl Vogt CH-1211 Geneva 4.

Experimental Section

Chemicals. GSH was purchased from Sigma. Synthesis and characterization of the molecule L^{3S} was previously described.[1] L^{3S} was dissolved in HEPES buffer (10 mM, pH 7.5) / acetonitrile, 6/4, v/v.

AgNP synthesis. 20 nm diameter AgNPs coated with citrate were synthesized based on [2]. Briefly, AgNPs were produced by reduction of $AgNO_3$ by tannic acid in presence of citrate. An aqueous solution (100 mL) containing 2 mM sodium citrate and 50 nM tannic acid were heated at 90 °C under 800 rpm stirring. When this temperature was reached five sequential additions of $AgNO_3$ (200 µL) at 25 mM were done every 5 min. Upon AgNP synthesis the solution becomes yellow. AgNPs are finally recovered by 1 hour centrifugation at 9000 g. The pellet containing AgNPs was washed twice with an aqueous solution of 2 mM sodium citrate.

AgNP assembly process. AgNPs at a final concentration of 370 µM in Ag were mixed in HEPES-Citrate buffer (10 mM HEPES, 2 mM sodium citrate pH 7) with L^{3S} at various concentrations in order to reach S:Ag molar ratio of 1:1, 0.25:1 or 0.05:1. The solutions were then incubated at 22 °C, under 400 rpm stirring for the desired incubation time before Ag quantification, AgNP SPR signal or DLS measurements. The process was also followed by AF_4-ICP-MS. All these analyses were performed as described in [3]. The experiments performed with GSH and GSSG were done using the same protocol according to S:Ag ratio mentioned in the different figure legends.

AgNP assembly production. For large scale assembly production, a S:Ag molar ratio of 0.25:1 was chosen. After 90 min reaction at 22 °C, the reaction was stopped by addition of 100 µM iodoacetamide. The mixture was further incubated in the same conditions for 2 hours. Assembly populations of different average diameters were fractionated over discontinuous gradient centrifugation made of 50 µL of buffer containing 1.5 M sucrose, 100 µL with 1.15 M sucrose, 200 µL with 0.9 M sucrose and 200 µL with 0.7 M sucrose, on top of which assembly mixtures (500 µL) were loaded. The gradient was centrifuged 20 min at 4400 g at 4 °C. Assemblies of different sizes were visually identified by their different colors and recovered by

pipetting layer by layer. Assemblies of average DLS diameter of 40, 60 and 200 nm were thus obtained. Each population of assemblies were then rinsed three times in HEPES-Citrate buffer by centrifugation.

Scanning transmission electron microscopy. Sample (5 µL) was deposited on a glow-discharged nickel grid coated with a carbon film (Mesh 300, Agar Scientific / S160N3) to avoid particle agglomeration and enable even dispersion of objects on the grid. The drop was then dried under air. STEM micrographs were taken on a Zeiss MERLIN microscope operated at 30 kV, using the solid-state bright-field detector. Micrographs were analyzed in the Fiji software.[4] For each sample, the number of NPs per assemblies was determined with a total counting of at least 600 individual NPs.

Cryo-transmission electron microscopy. A small volume (2-4 µL) of the sample was deposited on a glow-discharged holey carbon grid and vitrified using an FEI Vitrobot. Frozen grids were observed on an FEI F20 Tecnai microscope at 200 kV and images were recorded on an FEI Ceta detector.

Synchrotron radiation X-ray photoelectron spectroscopy. Synchrotron radiation X-ray Photoelectron Spectroscopy (SR-XPS) experiments were carried out at the BACH (Beamline for Advanced DiCHroism) beamline at the ELETTRA synchrotron facility (Basovizza, IT). XPS data were collected in fixed analyzer transmission mode (pass energy = 30 eV). A photon energy (PE) of 596 eV was used to acquire C 1s, S 2p, Ag 3d, O 1s and N 1s core-levels. The achieved resolving power was of 0.22 eV. Calibration of the energy scale was made by referencing to the gold Fermi-edge, and the metallic Ag $3d_{5/2}$ signal was always found at 368.20 eV, as expected.[5] XPS data analysis of S 2p and Ag 3d experimental spectra was performed via curve-fitting, by using a combination of Gaussian peaks, after subtraction of a Shirley background. The S $2p_{3/2}$ - S $2p_{1/2}$ and Ag $3d_{5/2}$ - Ag $3d_{3/2}$ doublets were fitted by using the same FWHM (full width half maximum) for the two spin-orbit components of the same signal, a spin-orbit splitting of 1.2 eV for S 2p and 6.0 eV for Ag 3d, and branching ratios S $2p_{3/2}$ / S $2p_{1/2}$ = 2, Ag $3d_{5/2}$ / Ag $3d_{3/2}$ = 3/2, respectively. In case of identifying presence of many chemically different species of the same element, the same FWHM

value was used for all individual photoemission bands in order to reduce the number of refinement parameters then improving the reliability of the results.

Time-of-Flight Secondary Ion Mass Spectroscopy. ToF-SIMS analysis was carried out at Université Claude Bernard-Lyon 1 (Villeurbanne, France) using a Physical Electronics TRIFT III ToF-SIMS instrument operated with a pulsed 22 keV Au^+ ion gun (ion current of 2 nA) rastered over a 300 µm x 300 µm area. Ion dose was kept below the static conditions limit. Data were analysed using the WinCadence™ software. Mass calibration was performed using hydrocarbon secondary ions.

Zêta potential. Zêta potential measurements were performed in a ZetaSizer (Malvern) at a 0.1 $g.L^{-1}$ silver concentration in DTS1060 cuvettes (Malvern) and at 25 °C. The final value is based on 200 acquisitions using the Smoluchowski model.[6]

Biocide assays. The *E. coli* strain K12 1655 was grown overnight in MD minimal medium (3.07 mM K_2HPO_4, 1.57 mM KH_2PO_4, 7.57 mM $NH_4(SO_4)_2$, 1.94 mM sodium citrate, 0.1 $g.L^{-1}$ glucose, 0.1 $g.L^{-1}$ magnesium sulfate, pH 7.4). For MIC determination, *E. coli* cells were then inoculated at 0.01 OD in 96-well plates in which assemblies or AgNPs were added in conditions allowing to screen for a wide range of Ag concentration. The plates were incubated at 37 °C with 900 rpm shaking in a Tecan reader plate and bacterial growth was continuously followed by measuring absorbance at 600 nm every 15 min. For *B. subtilis* (strain 3610), the set up was similar except that bacterial cells were grown in LB media. Besides, growth delays were determined instead of MIC that require too high Ag concentration.

Hepatocyte culture and cytotoxicity. HepG2 cells were grown in MEM media supplemented with fetal calf serum, glutamine and antibiotics (penicillin/streptomycin) and exposed to citrate-coated AgNPs or assemblies at the indicated concentrations of total Ag and for 24h. After exposure, HepG2 cells were harvested, suspended in PBS and mixed in one volume of Trypan Blue. Total and viable cells were counted in a TC20 Automated Cell Counter (Bio-Rad).

Supplementary figures

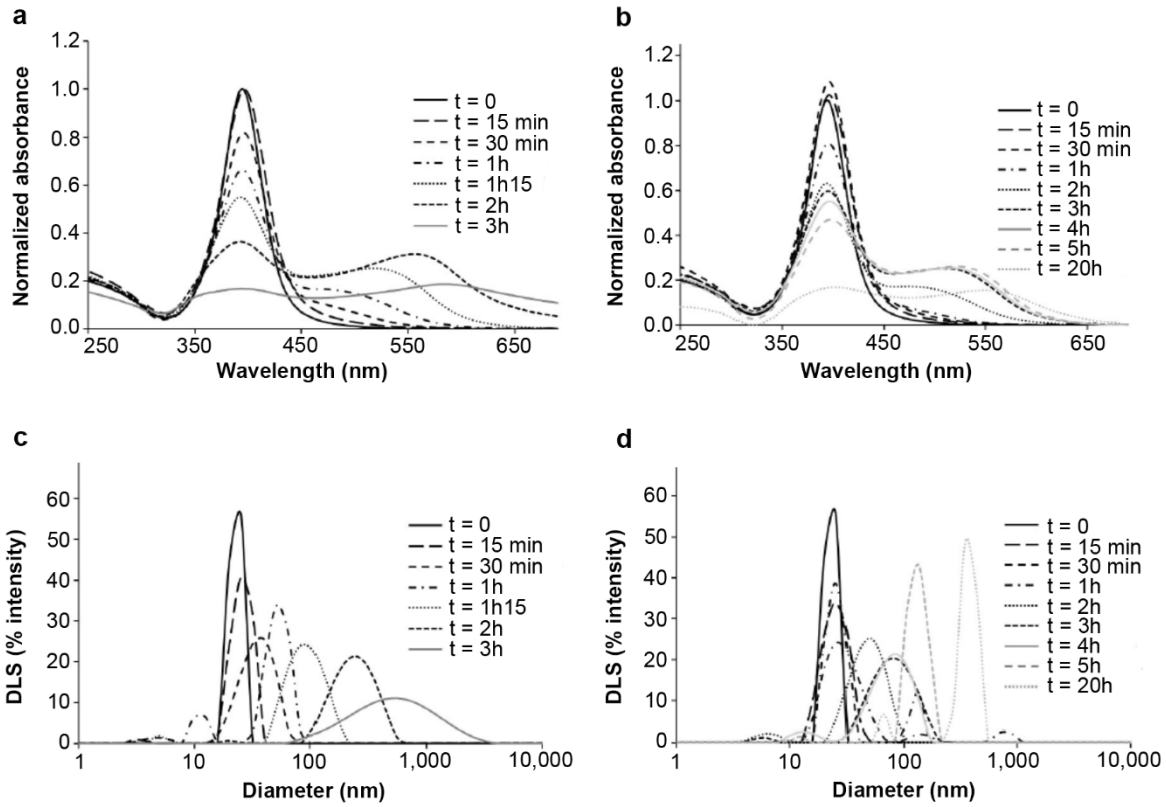

Fig. S1. L^{3S} -induced AgNP assemblies at various S:Ag ratio. (a) time-dependent analysis of AgNP SPR spectra in the presence of L^{3S} between 0 and 3 hours of incubation in 0.25:1, S:Ag molar ratio. (b) time-dependent analysis of AgNP SPR spectra in the presence of L^{3S} between 0 and 20 hours of incubation in 0.05:1, S:Ag molar ratio. (c) time-dependent evolution of the hydrodynamic diameter distribution of the species in a solution containing AgNP and L^{3S} at a 0.25:1, S:Ag molar ratio and between 0 and 3 hours of incubation. (d) time-dependent evolution of the hydrodynamic diameter distribution of the species in a solution containing AgNP and L^{3S} at a 0.05:1, S:Ag molar ratio and between 0 and 20 hours of incubation. In all experiments, t=0 corresponds to AgNPs alone in solution.

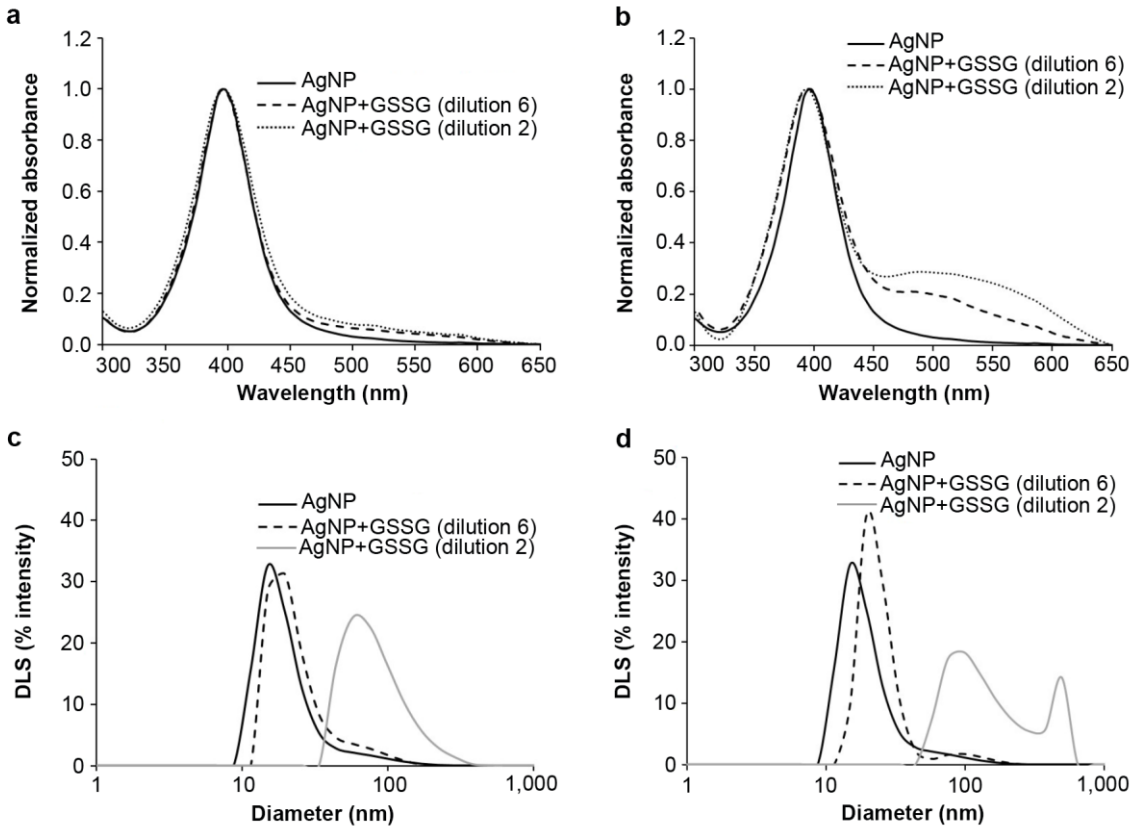

Fig. S2. AgNP agglomeration induced by oxidized glutathione. (a) AgNPs were incubated with oxidized glutathione (GSSG) for 30 min (a, c) or 1 hour (b, d) in presence of iodoacetamide (100 µM). The mixtures are then analyzed diluted two or six fold. SPR spectra of the different samples were recorded (a, b) and showed the appearance of higher wavelengths peaks in presence of GSSG that are partially lost upon 6-fold dilution. Hydrodynamic diameter distribution of the species in solution (c, d) showed the formation of large size species in presence of GSSG that are lost upon 6-fold dilution. GSSG induces the agglomeration of AgNPs. The optical properties of agglomerates are similar to those of assemblies but agglomerates are unstable upon dilution contrary to assemblies. The reaction have been performed at a 0.25:1, S:Ag molar ratio. Besides, the reactions were performed in presence of iodoacetamide to prove that this agglomeration is independent of reduced thiolate. “dilution 2” and “dilution 6” stands for 2-fold and 6-fold dilution of the sample, respectively.

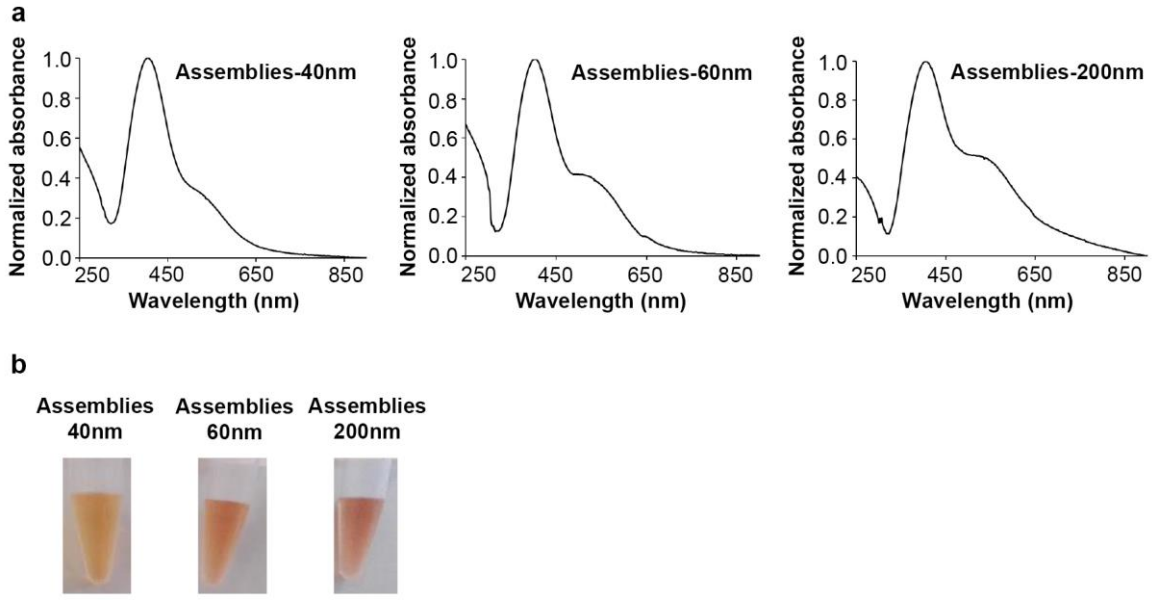

Fig. S3. Characterization of the different populations of assemblies. SPR spectra (a) and picture of the solution (b) of the different population of assemblies.

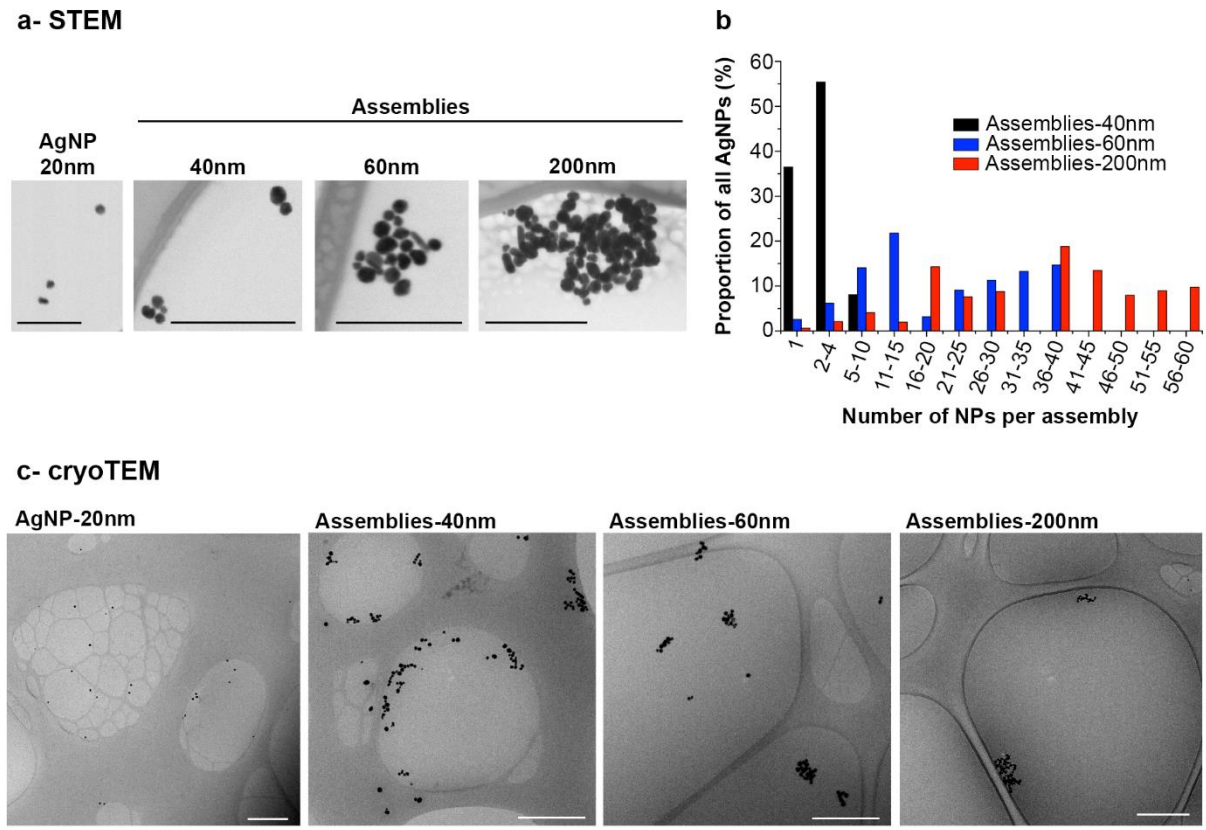

Fig. S4. Electron microscopy characterization of the different assemblies. (a) representative STEM micrographs of AgNPs alone and of the different populations of assemblies. Scale bars correspond to 200 nm. (b) statistical analysis of the number of particles per assembly in the different populations of assemblies based on STEM micrographs. The percentage of the total number of AgNP counted for an assembly population is given for each fraction. For each assembly population, at least 600 NPs have been counted. (c) large field cryo-TEM micrographs of AgNPs alone and of the different populations of assemblies. Scale bars correspond to 500 nm.

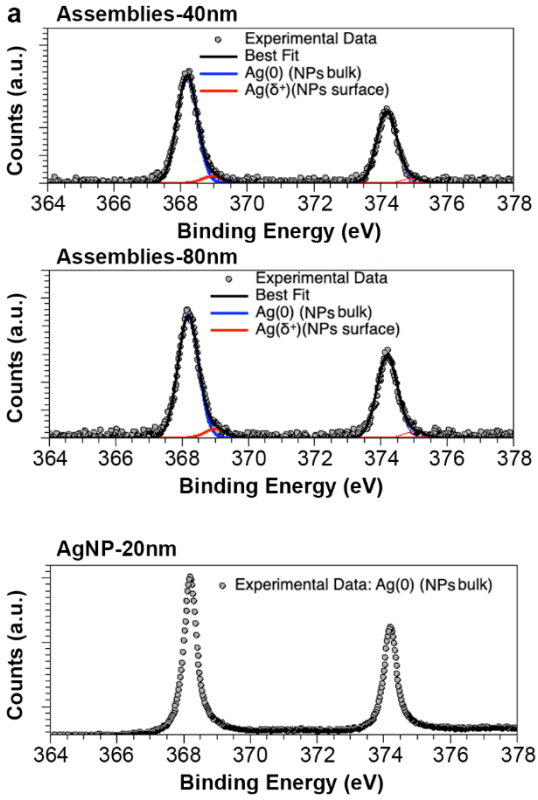

b

Assemblies	$Ag3d_{5/2}$ BE (eV)	FWHM (ev)	Atomic %*	Assignment
40 nm	368.20	0.71	93.4	Ag(0)
	368.96	0.71	6.6	$Ag(\delta^+)$
80 nm	368.20	0.73	93.2	Ag(0)
	369.02	0.73	6.8	$Ag(\delta^+)$

Fig. S5. Ag 3d XPS analysis. (a) SR-XPS Ag 3d core level spectra of 40 nm assemblies, 80 nm assemblies, and unassembled AgNPs of 20 nm diameter. AgNP assemblies show two pairs of spin-orbit components (Ag $3d_{5/2}$ and Ag $3d_{3/2}$, with intensity ratio Ag $3d_{5/2}$ / Ag $3d_{3/2}$ = 3/2, and doublet separation of 6.0 eV). Spectral assignments are based on Ag $3d_{5/2}$ component BE values. The main signal (Ag $3d_{5/2}$ = 368.2 eV, red curves) is attributed to metallic silver atoms at the NP core, while the signal at higher BE values (Ag $3d_{5/2}$ = 369.0 eV, blue curves) is due to partially positively charged silver atoms at the NP surface, $Ag(\delta^+)$, chemically interacting with thiol end-groups of the ligand L^{3S}.[5,7] (b) semiquantitative analysis and spectral assignment. * the statistic error in semiquantitative XPS analysis is of about 5% of the estimated value.[8]

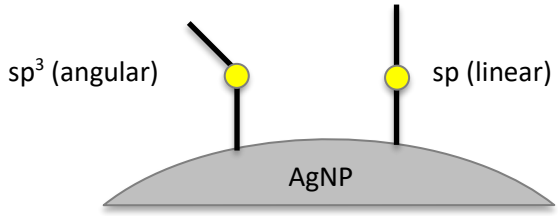

Scheme S1. Schematic representation of sulfur atoms (yellow circles) interacting with the Ag atoms on the nanoparticle surface in sp and sp^3 hybridizations.

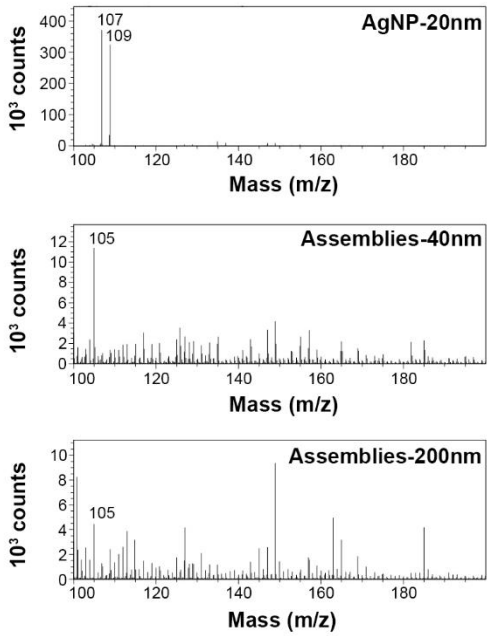

Fig. S6. Tof-SIMS analysis. ToF-SIMS positive mode spectra of AgNPs and of 40 and 200 nm assemblies in the m/z range of 100-200. Each sample was deposited on a mica slide and analyzed by ToF-SIMS. Ag was only detected for the AgNP sample as Ag^+ (peak at 107 and 109).

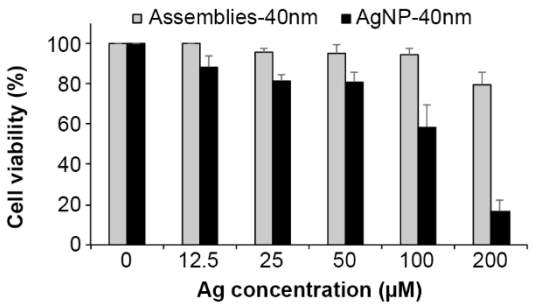

Fig. S7. Comparison of the toxicity of 40 nm AgNPs and assemblies on hepatocytes. Hepatocyte cells were exposed to 40 nm citrate-coated AgNPs or assemblies of 40 nm for 24h before being harvested. Total and viable cells were counted in a TC20 Automated Cell Counter (Bio-Rad) and using Trypan Blue.

Supplementary references

1 A. M. Pujol, C. Gateau, C. Lebrun and P. Delangle, *J. Am. Chem. Soc.*, 2009, **131**, 6928–6929.

2 N. G. Bastús, F. Merkoçi, J. Piella and V. Puntes, *Chem. Mater.*, 2014, **26**, 2836–2846.

3 M. Marchioni, T. Gallon, I. Worms, P.-H. Jouneau, C. Lebrun, G. Veronesi, D. Truffier-Boutry, E. Mintz, P. Delangle and A. Deniaud, *Environ. Sci. Nano*, 2018, **5**, 1911–1920.

4 J. Schindelin, I. Arganda-Carreras, E. Frise, V. Kaynig, M. Longair, T. Pietzsch, S. Preibisch, C. Rueden, S. Saalfeld, B. Schmid, J.-Y. Tinevez, D. J. White, V. Hartenstein, K. Eliceiri, P. Tomancak and A. Cardona, *Nat. Methods*, 2012, **9**, 676–682.

5 A. V. Naumkin, A. Kraut-Vass, S. W. Gaarenstroom and C. J. Powell, *NIST*, 2013.

6 A. Sze, D. Erickson, L. Ren and D. Li, *J. Colloid Interface Sci.*, 2003, **261**, 402–410.

7 I. Venditti, G. Testa, F. Sciubba, L. Carlini, F. Porcaro, C. Meneghini, S. Mobilio, C. Battocchio and I. Fratoddi, *J. Phys. Chem. C*, 2017, **121**, 8002–8013.

8 J. E. Castle, *Surf. Interface Anal.*, 1984, **6**, 302–302.